Do RadioAstron detections correlate with flaring states? An initial study of seven southern AGN

P.G. Edwards [a,*], J. Stevens [a], C. Phillips [a], C. Reynolds [a], Y.Y. Kovalev [b,c,d], P. Voitsik [b]
K. Sokolovsky [b,e,f], J. McCallum [g], J. Quick [h], R. Ojha [i,j]

[a] *CSIRO Astronomy and Space Science, PO Box 76, Epping, NSW 1710, Australia*
[b] *Astro Space Center of Lebedev Physical Institute, Profsoyuznaya St. 84/32, 117997 Moscow, Russia*
[c] *Institute of Physics and Technology, Dolgoprudny, Institutsky per., 9, Moscow region 141700, Russia*
[d] *Max-Planck-Institut für Radioastronomie, Auf dem Hügel 69, 53121 Bonn, Germany*
[e] *Sternberg Astronomical Institute, Moscow State University, Universitetskii pr. 13, 119992 Moscow, Russia*
[f] *Department of Physics and Astronomy, Michigan State University, East Lansing, 48824 Michigan, USA*
[g] *School of Physical Sciences, University of Tasmania, Private Bag 37, Hobart, TAS 7001, Australia*
[h] *SARAO, Hartebeesthoek Radio Astronomy Observatory, Krugersdorp 1740, South Africa*
[i] *NASA, Goddard Space Flight Center, Greenbelt, MD 20771, USA*
[j] *Catholic University of America, Washington, DC 20064, USA*

Abstract

We examine the state of seven southern radio sources at the time of their RadioAstron AGN Survey observations. Both ATCA flux density monitoring data and Fermi light-curves are considered in determining the relative activity of the source. A simple hypothesis, that sufficiently compact source structure exists for detections on RadioAstron baselines when the source is in a flaring state, is qualitatively tested. We find four instances of RadioAstron detections during flaring radio states and four instances of RadioAstron non-detections during fading or quiescent radio states, in support of the hypothesis. However, we also find three instances of RadioAstron detections during quiescent or fading radio states, and two non-detections during a flaring state, indicating that the situation is (not unexpectedly) more complex. Radio and gamma-ray monitoring such as that described here, together with the full RadioAstron AGN Survey results, will allow a more thorough investigation of the dependencies of detections on baselines of >10 Earth diameters.

1. Introduction

The RadioAstron space VLBI (Very Long Baseline Interferometry) mission has been conducting observations of compact radio sources on baselines up to 28 Earth diameters (E_D) since 2011 (Kardashev et al., 2013; Kardashev et al., 2017). The Spektr-R spacecraft is in a ~9 day lunar-perturbed orbit with apogee heights up to ~350,000 km, enabling unprecedented angular resolutions in the 0.327, 1.6, 4.8 and 22 GHz bands. Imaging observations can be carried out near perigee, and fringe-detection observations can be made throught the orbit.

The RadioAstron AGN Survey (Kovalev et al., 2020) is a survey of over 250 compact Active Galactic Nuclei (AGN). Some sources have been detected on >20 Earth diameter baselines, but many have not, and it is interesting to consider whether there are sources that have persistent

compact structure, sufficient to be always detectable on >10 E_D baselines, or whether RadioAstron detections on long baselines depend on the activity state of the source (i.e., whether it is flaring, fading, or quiescent). Naturally, other factors, such as the RadioAstron beam Position Angle relative to the jet PA of the source, radio spectral index, apparent jet speed, evidence of interstellar scintillation, sensitivity of the ground array etc., will also be of importance.

Kovalev et al. (2009) have noted that the GeV flux correlates well with the quasi-simultaneously measured compact radio flux density, and Valtaoja and Terasranta (1995) observed early in the EGRET mission that gamma-rays are generally detected when a quasar is in the initial phases of a high radio frequency outburst. The LAT (Large Area Telescope) instrument aboard the Fermi Gamma-ray Space Telescope has monitored the entire sky at GeV energies for over a decade (e.g. Acero et al., 2015). Preliminary weekly (and daily) fluxes of sources that have crossed a threshold of 1×10^{-6} photons/cm^2/s are made publicly available[1] to expedite multi-wavelength studies of flaring sources. All sources studied here are included in this list of monitored AGN and these Fermi-LAT lightcurves have been used to determine their level of activity in the GeV band. We will generate LAT lightcurves for our future, more detailed, investigations.

The Australia Telescope Compact Array is being used for two programs which are adding to long-term radio light-curves of AGN: the Observatory-led flux density calibration monitoring program (C007) and a multi-frequency program monitoring Fermi gamma-ray sources (C1730) (Stevens et al., 2012). Prior to 2009, C1730 observations were made with 128 MHz bandwidths centred at 4.8 & 8.6, 18.5 & 19.5 GHz. Observations at 38 & 40 GHz commenced in early 2007. Following the Compact Array Broadband Backend (CABB: Wilson et al., 2011) upgrade in 2009, C1730 observations are made with 2 GHz bandwidths centred at 5.5 & 9, 17 & 19, and 38 & 40 GHz. The observations are made in snap-shot mode, with integrations of several minutes in each pair of bands, and PKS 1934–638 is used as primary flux density calibrator. Errors are dominated by systematic effects and are estimated to be less than 5% below 10 GHz, and up to 10% at higher frequencies. We focus here on the 5.5 and 9.0 GHz data sets, as these frequencies were observed most often.

The sources considered here have been, or are being, monitored by ground-based VLBI monitoring programs, principally the 15 GHz MOJAVE program (Lister et al., 2009; Lister et al., 2016) for more northern sources and the 8 and 22 GHz TANAMI program (Ojha et al., 2010; Müller et al., 2018) for southern sources, providing information on the evolution of their parsec-scale morphologies. Radio flares often signal the emergence of a new, compact

component from the core, with implications for the detection on RadioAstron baselines.

Here, we examine RadioAstron detections as a function of ATCA and Fermi monitoring light curves to test the simple hypothesis that RadioAstron detections are more likely when an AGN is in a flaring or high state. A significant increase in radio flux density often presages the emergence of a new, compact component from the core, which is often preceded by a gamma-ray flare consistent with the formation of a shock region closer to the supermassive black hole. Similar considerations have been made for individual sources previously (Kovalev et al., 2016; Bruni et al., 2017; Edwards et al., 2017; Lisakov et al., 2017; Kutkin et al., 2018; Pilipenko et al., 2018). The seven sources considered in this paper are listed in Table 1. In the following sections we eschew the more traditional ordering by Right Ascension and consider the sources in turn in a more pedagogical ordering.

2. Observations

2.1. PKS 0727–115

Although PKS 0727–115 is undersampled in our ATCA monitoring, two prominent peaks in the light curve are evident (Fig. 1) and are confirmed with higher cadence radio monitoring provided by F-GAMMA (Fuhrmann et al., 2016). This is matched in the Fermi weekly light curves, however whereas the peaks have similar heights in the radio the first GeV peak in 2009/10 has flux levels twice that of the second peak around 2016. The source was monitored by MOJAVE from 2003 to 2012, and found to be highly core-dominated, with no component motion determined.

Due to its favorable position, close to the orbit apogee direction, PKS 0727–115 has been observed over 30 times with RadioAstron and detected in the majority of (but not all) epochs. We defer a full consideration of all epochs to a later publication, and consider here several illustrative epochs. A number of detections were made in 2013, during the onset of the second radio outburst, including detections

Table 1

Details of the RadioAstron observation of the sources considered in this paper. The designation L+ denotes the detection of fringes on baselines to Spektr-R at L-band (1.6 GHz), and C– the non-detection of space fringes at C-band (4.8 GHz), etc. (Kovalev et al., 2020). TANAMI and MOJAVE denote inclusion in that ground-based VLBI monitoring program: see text for details.

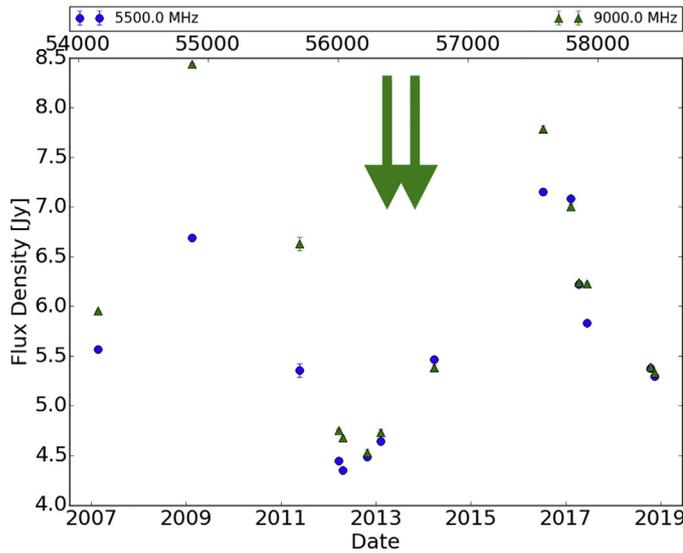| Source	RadioAstron Obs	VLBI
PKS 0208–512	L+C–	TANAMI
PKS 0454–234	L+C+ K+	MOJAVE
PKS 0516–621	L+C+	TANAMI
PKS 0537–441	L– C–	TANAMI
PKS 0727–115	L+C+ K+	MOJAVE
PKS 1424–418	L+C+	TANAMI
PKS 1622–253	L– C–	MOJAVE

Fig. 1. ATCA light-curve for PKS 0727–115. The green arrows indicate the epochs of the RadioAstron detections considered in the text. The numbers at the top of the plot are Modified Julian Date (MJD). (For interpretation of the references to colour in this figure legend, the reader is referred to the web version of this article.)

on baselines up to 11 E_D at L- and C-band, and detections at K-band on 2.4 E_D baselines to the GBT. These are consistent with our model of RadioAstron detections during active states.

2.2. PKS 1424–418

The ATCA lightcurve for PKS 1424–418 is dominated by a large outburst peaking in 2013/14 (Fig. 2). The Fermi weekly monitoring is also dominated by this flare, with several smaller flares evident in subsequent years. A possible

coincidence between the prominent radio and GeV outbursts and the detection of a PeV neutrino by the IceCube experiment was described by Kadler et al. (2016). Although the large uncertainty in the neutrino arrival direction precluded a definitive association, the plausible connection provides a model for testing source activity levels with future PeV neutrino events.

The AGN was observed three times by RadioAstron in 2014 March, close to the second peak of the radio outburst. The source was detected on 10 E_D baselines in raks01wh on 2014 March 19, but not on 13 or 20 E_D baselines in the other observations. The detection is consistent with our model of RadioAstron detections during active states: the contemporaneous non-detections will help constrain the size (or brightness temperature) of the most compact structure, and also indicate that a flaring state is no guarantee of a detection on the longest RadioAstron baselines.

2.3. PKS 0537–441

The ATCA light curve for PKS 0537–441 shows the source reached historical high levels in 2011/12 but has since declined from over 10 Jy to ∼2 Jy. The Fermi light curve shows similar behaviour, with high levels in the first 4 years of the mission but lower levels since then. A first-epoch TANAMI image from 2007 Nov 10 was presented by Ojha et al. (2010), with a derived brightness temperature of 1.1×10^{14} K — the highest of the 43 sources considered in that paper.

Fringes were not detected on ∼11 E_D RadioAstron baselines during raks01vb on 2014 Mar 04, when the source was in a fading state (Fig. 3): consistent with our model.
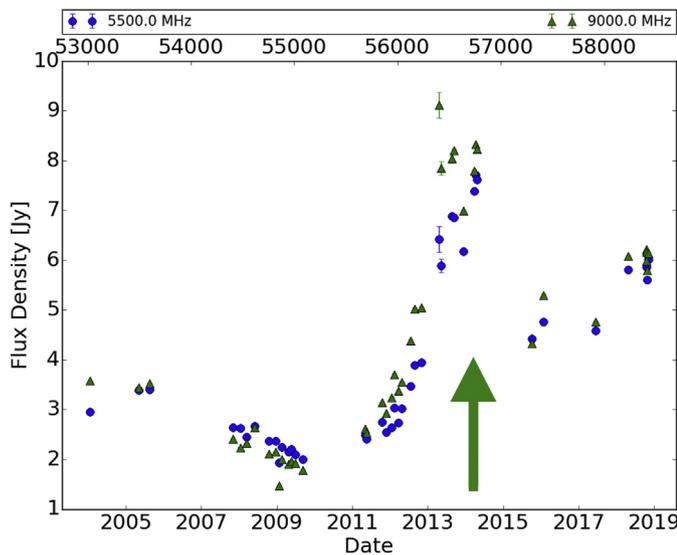

Fig. 2. ATCA light-curve for PKS 1424–418. The green arrow indicates the epoch of the RadioAstron detection considered in the text. The numbers at the top of the plot are MJD. (For interpretation of the references to colour in this figure legend, the reader is referred to the web version of this article.)
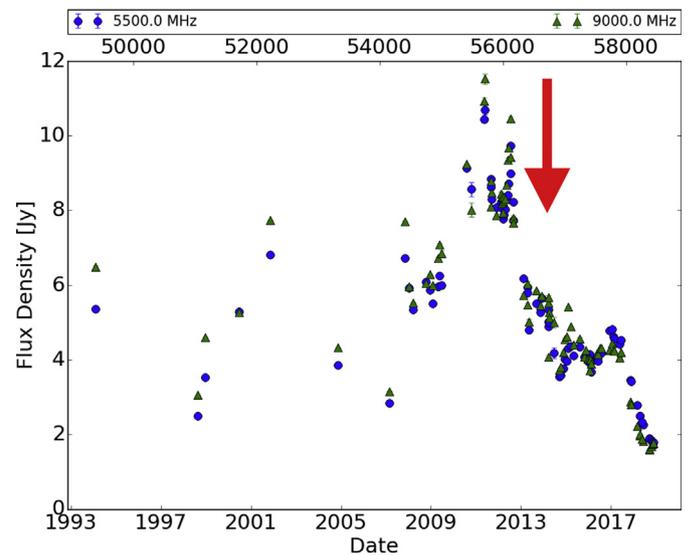

Fig. 3. ATCA light-curve for PKS 0537–441. The red arrow indicates the epoch of the RadioAstron non-detection considered in the text. The numbers at the top of the plot are MJD. (For interpretation of the references to colour in this figure legend, the reader is referred to the web version of this article.)

2.4. PKS 1622–253

PKS 1622–253 was detected on Earth–space baselines as part of the VSOP mission (Nakagawa et al., 2005) and was monitored as part of the MOJAVE project between 2009 and 2012. While a slight extension to the core is visible, no component motion has been determined for the source.

Fermi weekly light-curves reveal a bright outburst from the source in mid-2011, and a shortlived flare in late 2013, but a more quiescent state since then. Those two GeV high states correspond to the early stages of radio flares (i.e., the peaks of the radio outbursts lag the gamma-ray).

PKS 1622–253 has been observed twice during the RadioAstron mission, in raes03oi on 2013 March 14 and raks12sb on 2016 Mar 20, with no detection on the >18 E_D baselines of those two epochs. The ATCA light curve is under-sampled at the first epoch (Fig. 4), but it appears more likely the source was in a fading state (as the otherwise more precipitous drop in flux density would be probably be unprecedented). The second epoch is also undersampled, but with the available data the source appears to be in a relatively steady or quiescent state. With these caveats, the RadioAstron non-detections in fading or quiescent states curves is in keeping with our hypothesis.

2.5. PKS 0454–234

PKS 0454–234 is part of the MOJAVE program, with an apparent jet speed of ∼15 c reported for a single component (Lister et al., 2016). The Fermi weekly light curve shows the variable emission that characterises AGN at GeV energies, with two roughly year-long periods around MJD 55,500 and 58,000 of lower flux levels, which coincide with periods of quiescence in the ATCA monitoring. The radio light-curve is dominated by two peaks of similar heights at 9 GHz, but with differing spectral properties: the first peak has a more inverted spectrum whereas the second peak has a flatter spectrum between 5.5 and 9 GHz.

This source has been observed over 30 times as part of the RadioAstron mission (again, we defer a full consideration to a later paper), with the first detection taking place in raks08fk on 2014 Nov 9, on 13 E_D baselines. This was preceded by half a dozen observations, beginning on 2013 Sep 9, all of which had no detections on space baselines between 9 and 17 E_D. It is apparent from Fig. 5 that these non-detections, indicated by the red arrow, were made while the flux density of the source was decreasing, with the first detection, indicated by the first green arrow, coming after the source had started to brighten, in keeping with our simple model.

However, the longest baselines the source has been detected on to date are 23 E_D during raks16bk on 2016 Oct 20, on baselines to Parkes. At this time, the source had decreased significantly from its peak and was in a fading state, in contrast to our hypothesis.

2.6. PKS 0516–621

Ground-based VLBI observations of PKS 0516–621 are reported by Edwards et al. (2018) (epoch 2001 Nov 10) and Müller et al. (2018) (epoch 2009 Feb 23). At both epochs the source appeared as a single component with a brightness temperature of ∼3.5 × 10^{11} K.

The source was detected on baselines of 10 E_D in raks08af on 2014 Aug 21, with this epoch indicated by the arrow in Fig. 6. It is apparent the source was in a decaying phase at this time, with the flux density having halved from
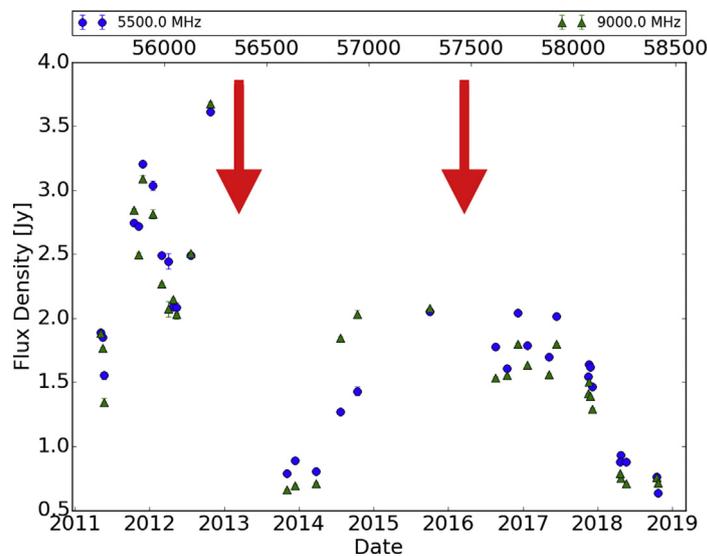

Fig. 4. ATCA light-curve for PKS 1622–253. The red arrows indicate the epochs of the RadioAstron non-detections considered in the text. The numbers at the top of the plot are MJD. (For interpretation of the references to colour in this figure legend, the reader is referred to the web version of this article.)
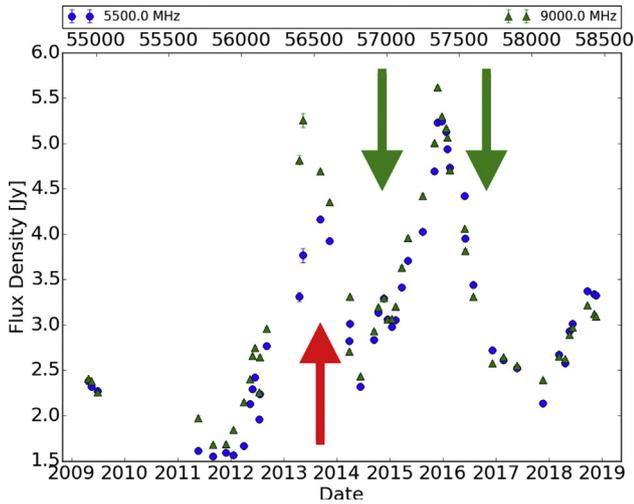
Fig. 5. ATCA light-curve for PKS 0454–234. The red and green arrows respectively indicate the epochs of the RadioAstron non-detections and detections considered in the text. The numbers at the top of the plot are MJD. (For interpretation of the references to colour in this figure legend, the reader is referred to the web version of this article.)

a year earlier. Again, this is not as our model would have predicted.

2.7. PKS 0208–512

PKS 0208–512 was detected on Earth-space baselines as part of the VSOP mission (Tingay et al., 2002) and is a bright GeV gamma-ray source. The first 8.4 GHz TANAMI observation, in 2007 Nov 10, yielded a brightness temperature of 6.2×10^{12} K (Ojha et al., 2010), and multi-epoch VLBI data suggest the source is highly superluminal, with an apparent speed of $\sim 20\,c$ (Edwards et al., 2018). As indicated in Fig. 7, PKS 0208–512 was in radio

high-state at the time of first TANAMI observation, and has been returning to those levels since 2016. The Fermi monitored source list light curves reveal GeV high states at similar times: in 2008, 2010, and since 2016.

PKS 0208–512 was detected on 9.8 E_D baselines as part of the AGN survey observation raks08bz on 2014 Oct 3. The flux density was in a slight decline at this time, suggesting a fading or quiescent state. Again, this is in contrast to our simplistic expectations.
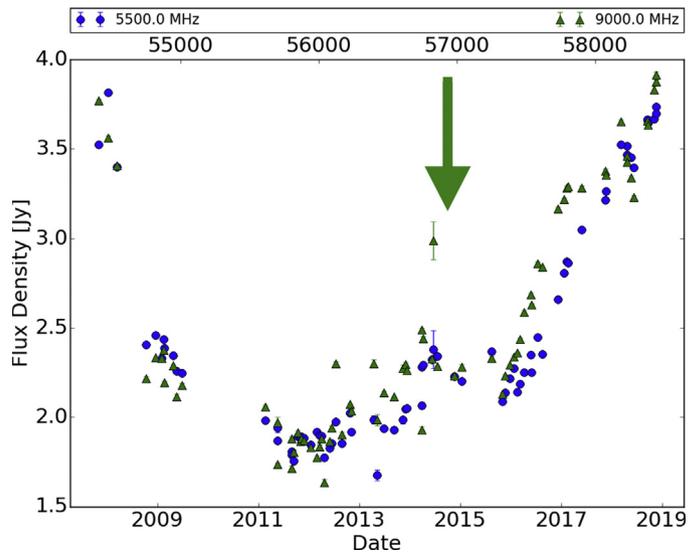

Fig. 7. ATCA light-curve for PKS 0208–512. The green arrow indicates the epoch of the RadioAstron detection considered in the text The numbers at the top of the plot are MJD. (For interpretation of the references to colour in this figure legend, the reader is referred to the web version of this article.)
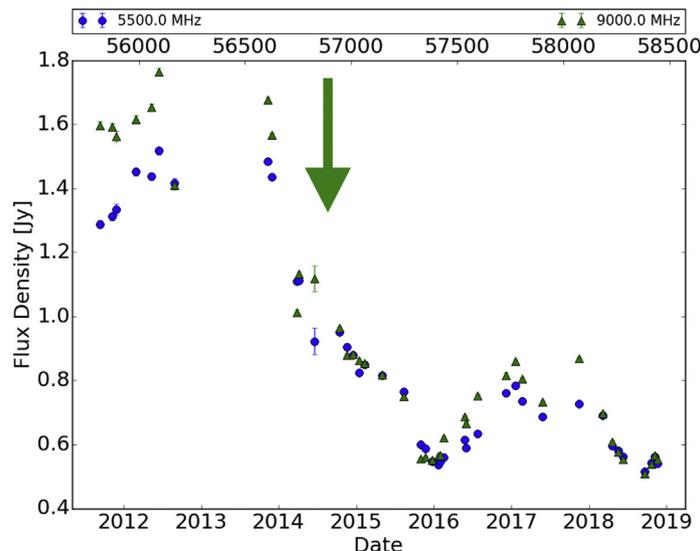

Fig. 6. ATCA light-curve for PKS 0516–621. The green arrow indicates the epoch of the RadioAstron detection considered in the text. The numbers at the top of the plot are MJD. (For interpretation of the references to colour in this figure legend, the reader is referred to the web version of this article.)

3. Conclusions

We have tested a hypothesis that RadioAstron detections on long baselines will be more likely when the source is in a flaring or high state in the radio or gamma-ray bands. Some support for this model is found in the RadioAstron detections of PKS 0727–115, PKS 1424–418 and PKS 0454–234 in flaring states; and from the RadioAstron non-detections of PKS 0537–441 and PKS 1622–253 in fading or quiescent states. However, observations of PKS 0454–234, PKS 0516–621 and PKS 0208–512 have demonstrated that RadioAstron AGN Survey detections can also be made in fading and quiescent states. Finally, RadioAstron non-detections of PKS 1424–418 during an on-going flaring state serve as a salutory reminder that other factors, such as projected baseline length, ground array sensitivity, and RadioAstron beam Position angle relative to the AGN jet Position Angle, are also of importance.

The small size of this sample precludes any attempt at meaningful statistical conclusions, but the examples given here, while indicating that the simplest hypothesis can be rejected, indicate the potential for a large study in the future. TANAMI, MOJAVE, and ATCA monitoring will complement other radio programs (e.g. Richards et al., 2014; Fuhrmann et al., 2016) and ongoing Fermi monitoring in studying the circumstances and parameters of RadioAstron detections.

Acknowledgements

References

Acero, F., Ackermann, M., Ajello, M., et al., 2015. Fermi large area telescope third source catalog. ApJS 218, 23.

Bruni, G., Gómez, J.L., Casadio, C., et al., 2017. Probing the innermost regions of AGN jets and their magnetic fields with RadioAstron. II. Observations of 3C 273 at minimum activity. A&A 604, A111.

Edwards, P.G., Kovalev, Y.Y., Ojha, R., et al., 2017. PKS 1954-388: RadioAstron detection on 80,000 km baselines and multiwavelength observations. PASA 34, 21.

Edwards, P.G., Ojha, R., Dodson, R., et al., 2018. VLBI observations of southern gamma-ray sources. III. PASA 35, 9.

Fuhrmann, L., Angelakis, E., Zensus, J.A., et al., 2016. The F-GAMMA programme: multi-frequency study of active galactic nuclei in the Fermi era. Programme description and the first 2.5 years of monitoring. A&A 596, A45.

Kadler, M., Krauß, F., Mannheim, K., et al., 2016. Coincidence of a high-fluence blazar outburst with a PeV-energy neutrino event. Nat. Phys. 12, 807–814.

Kardashev, N.S., Khartov, V.V., Abramov, V.V., et al., 2013. Radio-Astron — A telescope with a size of 300 000 km: main parameters and first observational results. ARep 57, 153–194.

Kardashev, N.S., Alakoz, A.V., Andrianov, A.S., et al., 2017. Radio-Astron science program five years after launch: main science results. Sol. Syst. Res. (7), 535–555

Kovalev, Y.Y., Aller, H.D., Aller, M.F., et al., 2009. The relation between AGN gamma-ray emission and parsec-scale radio jets. ApJL 696, L17–L21.

Kovalev, Y.Y., Kardashev, N.S., Kellermann, K.I., et al., 2016. Radio-Astron observations of the Quasar 3C273: a challenge to the brightness temperature limit. ApJL 820, L9.

Kovalev, Y.Y., et al. 2020. Detection statistics of the RadioAstron AGN survey. Adv. Space Res. 65(2), 705–711.

Kutkin, A.M., Pashchenko, I.N., Lisakov, M.M., et al., 2018. The extreme blazar AO 0235+164 as seen by extensive ground and space radio observations. MNRAS 475, 4994–5009.

Lipunov, V., Kornilov, V., Gorbovskoy, E., et al., 2010. Master robotic net. Adv. Astron. 2010, 349171.

Lisakov, M.M., Kovalev, Y.Y., Savolainen, T., Hovatta, T., Kutkin, A.M., 2017. A connection between -ray and parsec-scale radio flares in the blazar 3C 273. MNRAS 468, 4478–4493.

Lister, M.L., Cohen, M.H., Homan, D.C., et al., 2009. MOJAVE: monitoring of jets in active galactic nuclei with VLBA experiments. VI. Kinematics analysis of a complete sample of Blazar jets. AJ 138, 1874–1892.

Lister, M.L., Aller, M.F., Aller, H.D., et al., 2016. MOJAVE: XIII. Parsec-scale AGN jet kinematics analysis based on 19 years of VLBA observations at 15 GHz. AJ 152, 12.

Müller, C., Kadler, M., Ojha, R., et al., 2018. TANAMI: Tracking active galactic nuclei with austral milliarcsecond Interferometry. II. Additional sources. A&A 610, A1.

Nakagawa, A., Edwards, P.G., Murata, Y., Wajima, K., Modaka, T., 2005. VSOP Observations of the Gamma-Ray Sources J1733-1304, J1625-2527, and J1015+4926. PASJ 57, 295–308.

Ojha, R., Kadler, M., Böck, M., et al., 2010. TANAMI: Tracking active galactic nuclei with austral milliarcsecond interferometry I. First-Epoch 8.4 GHz Images. A&A 519, A45.

Pilipenko, S.V., Kovalev, Y.Y., Andrianov, A.S., et al., 2018. The high brightness temperature of B0529+483 revealed by RadioAstron and implications for interstellar scattering. MNRAS 474, 3523–3534.

Richards, J.L., Hovatta, T., Max-Moerbeck, W., et al., 2014. Connecting radio variability to the characteristics of gamma-ray blazars. MNRAS 438, 3058–3069.

Stevens, J., Edwards, P.G., Ojha, R., et al. 2012. In: Proc. Fermi and Jansky Conf. – eConf C111110, arXiv:<1205.2403>.

Tingay, S.J., Reynolds, J.E., Tzioumis, A.K., et al., 2002. VSOP space VLBI and geodetic VLBI investigations of southern hemisphere radio sources. ApJS 141, 311–335.

Valtaoja, E., Terasranta, H., 1995. Gamma radiation from radio shocks in AGN jets. A&A 297, L13–L16.

Wilson, W.E., Ferris, R.H., Axtens, P., et al., 2011. The Australia Telescope Compact Array Broadband Backend (CABB): description & first results. MNRAS 416, 832–856.